Am J Cancer Res 2015;5(9):2643-2659
www.ajcr.us /ISSN:2156-6976/ajcr0008500

Original Article

LIN28B suppresses microRNA let-7b expression to promote CD44+/LIN28B+ human pancreatic cancer stem cell proliferation and invasion

Yebo Shao[1*], Lei Zhang[1*], Lei Cui[2*], Wenhui Lou[1], Dansong Wang[1], Weiqi Lu[1], Dayong Jin[1], Te Liu[3]

[1]Department of General Surgery, Zhongshan Hospital, Fudan University, Shanghai 200032, China; [2]Department of General Surgery, Jiangsu University Affiliated Hospital, Zhengjiang 212000, China; [3]Shanghai Geriatric Institute of Chinese Medicine, Longhua Hospital, Shanghai University of Traditional Chinese Medicine, Shanghai 200031, China. [*]Equal contributors.

Received March 27, 2015; Accepted July 5, 2015; Epub August 15, 2015; Published September 1, 2015

Abstract: Although the highly proliferative, migratory, and multi-drug resistant phenotype of human pancreatic cancer stem cells (PCSCs) is well characterized, knowledge of their biological mechanisms is limited. We used CD44 and LIN28B as markers to screen, isolate, and enrich CSCs from human primary pancreatic cancer. Using flow cytometry, we identified a human primary pancreatic cancer cell (PCC) subpopulation expressing high levels of both CD44 and LIN28B. CD44+/LIN28B+ PCSCs expressed high levels of stemness marker genes and possessed higher migratory and invasive ability than CD44-/LIN28B- PCCs. CD44+/LIN28B+ PCSCs were more resistant to growth inhibition induced by the chemotherapeutic drugs cisplatin and gemcitabine hydrochloride, and readily established tumors *in vivo* in a relatively short time. Moreover, microarray analysis revealed significant differences between the cDNA expression patterns of CD44+/LIN28B+ PCSCs and CD44-/LIN28B- PCCs. Following siRNA interference of endogenous *LIN28B* gene expression in CD44+/LIN28B+ PCSCs, not only was their proliferation decreased, there was also cell cycle arrest due to suppression of cyclin D1 expression following the stimulation of miRNA let-7b expression. In conclusion, CD44+/LIN28B+ cells, which possess CSC characteristics, can be reliably sorted from human primary PCCs and represent a valuable model for studying cancer cell physiology and multi-drug resistance.

Keywords: Pancreatic ductal adenocarcinoma, cancer stem cells, CD44, Lin28B

Introduction

Pancreatic ductal adenocarcinoma (PDAC) is a highly lethal malignancy that is usually diagnosed at a late stage, at which optimal therapeutic options have been skipped [1]. It is one of the most chemoresistant tumors; the survival rate is < 5% [2]. PDAC is not only notorious for being difficult to diagnose at an early stage and its poor recurrence-free prognosis, but also the lack of effective treatment thereof and limited knowledge of its biological characteristics [3, 4]. Thus, there is an urgent need for better understanding of the cellular/molecular properties associated with PDAC to explore novel venues of diagnosis and treatment of this disease [1, 5, 6]. Recent evidence suggests that tumors consist of heterogeneous cell populations, which possess different biological properties; furthermore, the capacity for tumor formation and growth resides exclusively in a small proportion of tumor cells, termed cancer stem cells (CSCs) [7-11]. Pancreatic CSCs (PCSCs) were first characterized by Li et al. [6] and were shown to be not only highly tumorigenic, but also possessed the ability to self-renew and produce differentiated progeny that reflected the heterogeneity of the patient's primary tumor [3]. Moreover, an increasing number of studies have reported human pancreatic cancer cell subpopulations, such as CD31+/CD45+ [12]; Hoechst 33342-/CD133+/ALDH1+ [1]; ESA+/CD44+ [3]; and CD24+/CD44+ [4], which express CSC-associated characteristics and stem cell markers [5]. There are several prominent CSC characteristics: they (a) self-renew and are highly clonogenic, (b) differentiate *in vitro* to form organized spheroids in sus-

pension, (c) express multipotency and tissue-specific differentiation markers, (d) generate tumors *in vivo* through self-renewal mechanisms, (e) undergo *in vivo* differentiation to produce a disease similar to that in the patient [13]. The observation that stem cells and some CSCs share the common defining features of incompletely differentiated state and self-renewal capacity led to the CSC hypothesis as a possible mechanism for total tumor growth as the result of the proliferation of a small subpopulation of cells [9-11, 14].

LIN28, which is an RNA-binding protein, regulates cell growth and differentiation [15]. Developmental timing in *Caenorhabditis elegans* is regulated by a heterochronic gene pathway. The heterochronic gene *LIN28* is a key regulator early in the pathway [16]. *LIN28* encodes an approximately 25-kDa protein with two RNA-binding motifs: a so-called "cold shock domain" (CSD) and a pair of retroviral-type CCHC zinc fingers; it is the only known animal protein with this motif pairing. The CSD is a β-barrel structure that binds single-stranded nucleic acids [16]. LIN28 inhibits the biogenesis of a group of microRNAs (miRNAs), among which are the let-7 family miRNAs shown to participate in regulation of the expression of genes involved in cell growth and differentiation [17]. The mechanism underlying selective let-7 inhibition by LIN28 has been studied extensively. The common theme is that LIN28 binds to the terminal loop region of pri/pre-let-7 and blocks their processing [15]. The miRNAs are small RNA molecules (21-23 nucleotides) that act as negative regulators of gene expression either by blocking mRNA translation into protein or through RNA interference [18-21]. Previous studies have reported that dysregulation of specific miRNAs is associated with certain types of cancer, and they are thought to act as either oncogenes or tumor suppressors depending on the target gene [19, 21, 22]. Furthermore, the miRNA let-7b regulates self-renewal of embryonic stem cells and the proliferation and tumorigenicity of cancer cells by inhibiting cyclin D1 (CCND1) expression [23-25].

In view of the above findings, we sorted a novel CSC subpopulation overexpressing CD44 and LIN28B at the cell surface (CD44+/LIN28B+) from human primary pancreatic cancer tissues. We demonstrated a CD44+/LIN28B+ PCSC subpopulation that proliferates rapidly and exhibits multi-drug resistance, high invasion ability, and adherin. Therefore, CD44+/LIN28B+ PCSCs represent a potentially powerful *in vitro* model for studying cancer cell metastasis, invasion, and self-renewal and for assessing the effectiveness of novel therapeutics for PDAC.

Materials and methods

Isolation CD44 and LIN28B phenotype cells by magnetic activated cell sorting system

CD44+ and LIN28B+ subpopulation cells were isolated from primary cancer cells from pancreatic cancer tissues using 4 μl of the primary monoclonal antibodies (rabbit anti-human LIN28B-FITC, rabbit anti-human CD44-PE, eBioscience) stored at 4°C in PBS for 30 min in a volume of 1 ml as previously described [7, 21]. After reaction, the cells were washed twice in PBS, and were put the secondary monoclonal antibodies (Goat anti-rabbit coupled to magnetic microbeads, Miltenyi Biotec, Auburn, CA), incubated at 10°C in PBS for 15 min and then washed twice in PBS. Single cells were plated at 1000 cells/ml in DMEM: F12 (HyClone), supplemented with 10 ng/ml basic fibroblast growth factor (bFGF), 10 ng/ml epidermal growth factor (EGF), 5 μg/ml insulin and 0.5% bovine serum albumin (BSA) (all from Sigma-Aldrich). All CD44+/LIN28B+ cells were cultured in above conditions as non-adherent spherical clusters which were called PCSCs, and CD44-/LIN28B- cells which were cultured under general conditions as adherent clusters, was called PCCs. All Cells had been cultured on the same conditions until passage 4th before making ulterior experiments. The methods were carried out in accordance with the approved guidelines.

Quantitative Real-time PCR (qRT-PCR) analysis

Total RNA from each cells was isolated using Trizol Reagent (Invitrogen) according to the manufacturer's protocol. The RNA samples were treated with Dnase I (Sigma-Aldrich), quantified, and reverse-transcribed into cDNA using the ReverTra Ace-α First Strand cDNA Synthesis Kit (TOYOBO). qRT-PCR was conducted using a RealPlex4 real-time PCR detection system from Eppendorf Co. LTD (Germany), with SyBR Green RealTime PCR Master MIX

(TOYOBO) used as the detection dye. qRT-PCR amplification was performed over 40 cycles with denaturation at 95°C for 15 sec and annealing at 58°C for 45 sec. Target cDNA was quantified using the relative quantification method. A comparative threshold cycle (Ct) was used to determine gene expression relative to a control (calibrator) and steady-state mRNA levels are reported as an n-fold difference relative to the calibrator. For each sample, the maker genes Ct values were normalized using the formula ΔCt = Ct_markers-Ct_18sRNA. To determine relative expression levels, the following formula was used ΔΔCt = ΔCt_CSCs-ΔCt_CCs. The values used to plot relative expressions of markers were calculated using the expression $2^{-\Delta\Delta Ct}$. The mRNA levels were calibrated based on levels of 18 s RNA. The cDNA of each stem cell markers was amplified using primers as previously described [21].

Multi-chemodrugs resistant assay

The chemodrugs (casplatin, gemcitabine hydrochloride) resistant assay of each cell was completely performed as previously described [7, 21].

Western blotting analysis

Protein extracts of each cell were resolved by 12% SDS-PAGE and transferred on PVDF (Millipore) membranes. After blocking, the PVDF membranes were washed 4 times for 15 min with TBST at room temperature and incubated with primary antibody (rabbit anti-human LIN28B, rabbit anti-human CCND1 all from Cell Signaling Technology). Following extensive washing, membranes were incubated with secondary peroxidase-linked Goat anti- rabbit IgG (Santa Cruz) for 1 h. After washing 4 times for 15 min with TBST at room temperature once more, the immunoreactivity was visualized by enhanced chemiluminescence (ECL kit, Pierce Biotechnology).

Immunofluorescence staining analysis

The cultured cells were washed 3 times with PBS and fixed with 4% paraformaldehyde (Sigma-Aldrich, St. Louis, USA) for 30 min. After blocking, the cells were incubated first antibodies overnight at 4°C, and then with Cy3-conjugated goat anti-rabbit IgG antibody (1:200; Abcam, Cambridge, UK) and 5 μg/ml DAPI (Sigma-Aldrich) at room temperature for 30 min. Then the cells were thoroughly washed with TBST and viewed through a fluorescence microscope (DMI3000; Leica, Allendale, NJ, USA).

Soft agar colony formation assay

All steps were according to the previously described [19]. Soft Agar Assays were constructed in 6-well plates. The base layer of each well consisted of 2 mL with final concentrations of 1 × media (DMEM+10% FBS) and 0.6% low melting point agarose. Plates were chilled at 4°C until solid. Upon this, a 1.0 ml growth agar layer was poured, consisting of 1×10^4 cells suspended in 1 × media and 0.3% low melting point agarose. Plates were again chilled at 4°C until the growth layer congealed. An additional 1.0 ml of 1 × media without agarose was added on top of the growth layer on day 0 and again on day 15 of growth. Cells were allowed to grow at 37°C for 1 month and total colonies counted. Assays were repeated a total of 3 times. Results were statistically analyzed by paired T-test using the PRISM Graphpad program.

Transwell migration assay

All steps were according to the previously described [19]. Cells (2×10^5) were resuspended in 200 μl of serum-free medium and seeded on the top chamber of the 8.0 μm pore, 6.5 mm polycarbonate transwell filters (Corning). The full medium (600 μl) containing 10% FBS was added to the bottom chamber. The cells were allowed to migrate for 24 h at 37°C in a humidified incubator with 5% CO_2. The cells attached to the lower surface of membrane were fixed in 4% paraformaldehyde at room temperature for 30 mins and stained with 4,6-diamidino-2-phenylindole (DAPI) (C1002, Beyotime Inst Biotech, China), and the number of cells on the lower surface of the filters was counted under the microscope. A total of 5 fields were counted for each transwell filter.

In vivo xenograft experiments

About 1×10^4 cells (PCSCs or PCCs) were inoculated *s.c* in athymic nude mice. All mice of 6-7 weeks of age were carried out at Experimental Animal Center of Fudan University and Use Committer approval in accordance with institutional guidelines.

Northern blotting

Northern blotting was done as previously described [20]. For all cell treatment groups, 20 μg of good quality total RNA was analyzed on a 7.5 M urea, 12% PAA denaturing gel and transferred to a Hybond N+ nylon membrane (Amersham, Freiburg, Germany). Membranes were cross-linked using ultraviolet light for 30 s at 1200 mJ/cm^2 and hybridized to the let-7b antisense Starfire probe, 5'-AACCACACAACC-TACTACCTCA-3' (Sangon Biotech Co., Ltd, Shanghai, China) for the detection of 22-nt le7-7b fragments, according to the manufacturer's instructions. After washing, membranes were exposed to Kodak XAR-5 film for 20-40 h (Sigma-Aldrich Chemical). A human U6 snRNA probe (5'-GCAGGGGCCATGCTAATCTTCTCTGTAT-CG-3') was used as a positive control, with an exposure time of 15-30 min.

cDNA microarray analysis

Total RNAs of PCSCs and PCCs were labeled using Agilent's Low RNA Input Fluorescent Linear Amplification kit. Cy3-dCTP or Cy5-dCTP was incorporated during reverse transcription of 5 μg total RNAs into cDNA. Different fluorescently labeled cDNA probes were mixed in 30 μl hybridization buffer (3 × SSC, 0.2% SDS, 5 × Denhardt's solution and 25% formamide) and applied to the microarray (CapitalBio human mRNA microarray V2.0, CapitalBio, Beijing, China) following incubation at 42°C for 16 h. After hybridization, the slide was washed with 0.2% SDS/2 × SSC at 42°C for 5 min, and then was washed with 0.2 × SSC at room temperature for 5 min. The fluorescent images of the hybridized microarray were scanned with an Agilent Whole Human Genome 4 × 44 microarray scanner system (Santa Clara, CA, USA). Images and quantitative data of the gene-expression levels were analyzed by Agilent's Feature Extraction (FE) software, version 9.5.

Flow cytometric (FCM) analysis of cell cycle by PI staining

Each group cells were seeded at 3 × 10^5 per well in 6-well plates and cultured until 85% confluent. Each group cells was washed by PBS on three times, then were collected by centrifugation (Allegra X-22R, Beckman Coulter) at 1000 *g* for 5 min. The cell pellets were the resuspended in 1 mL of PBS, fixed in 70% ice-cold ethanol, and kept in a freezer more than 48 h. Before flow cytometric analysis, The fixed cells were centrifuged, washed twice with PBS, and resuspended in PI staining solution (Sigma-Aldrich Chemical) containing 50 μL/mL PI and 250 μg/mL RNase A (Sigma-Aldrich Chemical). The cell suspension, which was hidden from light, were incubated for 30 min at 4°C and analyzed using the FACS (FACSAria, BD Bioscience, CA, USA). A total of 20,000 events were acquired for analysis using CellQuest software.

Methyl thiazolyl tetrazolium (MTT) assay for cell proliferation

Each group cells was seeded at 2 × 10^3 per well in 96-well plates and cultrued in DMEM supplemented with 10% FBS at 37°C with 5% CO_2, until 85% confluent. MTT (Sigma Chemicals) reagent (5 mg/ml) was added to the maintenance cell medium at different time points, and incubated at 37°C for an additional 4 h. The reaction was terminated with 150 μL dimethylsulfoxide (DMSO, Sigma Chemicals) per well and the cells were lysed for 15 min, and the plates were gently shaked per 5 min. Absorvance values were determined by using the enzyme linked immunosorbent assay (ELISA) reader (Model 680, Bio-rad) at 490 nm.

Statistical analysis

Each experiment was performed as least three times, and data are shown as the mean ± SE where applicable, and differences were evaluated using Student's *t*-tests. The probability of $P < 0.05$ was considered to be statistically significant.

Results

CD44+/LIN2B+ PCSCs proliferated more rapidly and exhibited multi-drug resistance

We used a magnetic-activated cell sorting system to isolate and enrich the CD44- and LIN28B- overexpressing subpopulation from the primary tumor cells of four human pancreatic cancer tissues. After isolation, cells were quantified by flow cytometry (FCM). CD44+/LIN28B+ PCSCs represented 0.515% ± 0.105% of the total population in four primary pancreatic cancer cells, whereas CD44-/LIN28B-PCCs represented 91.581% ± 2.961% of the

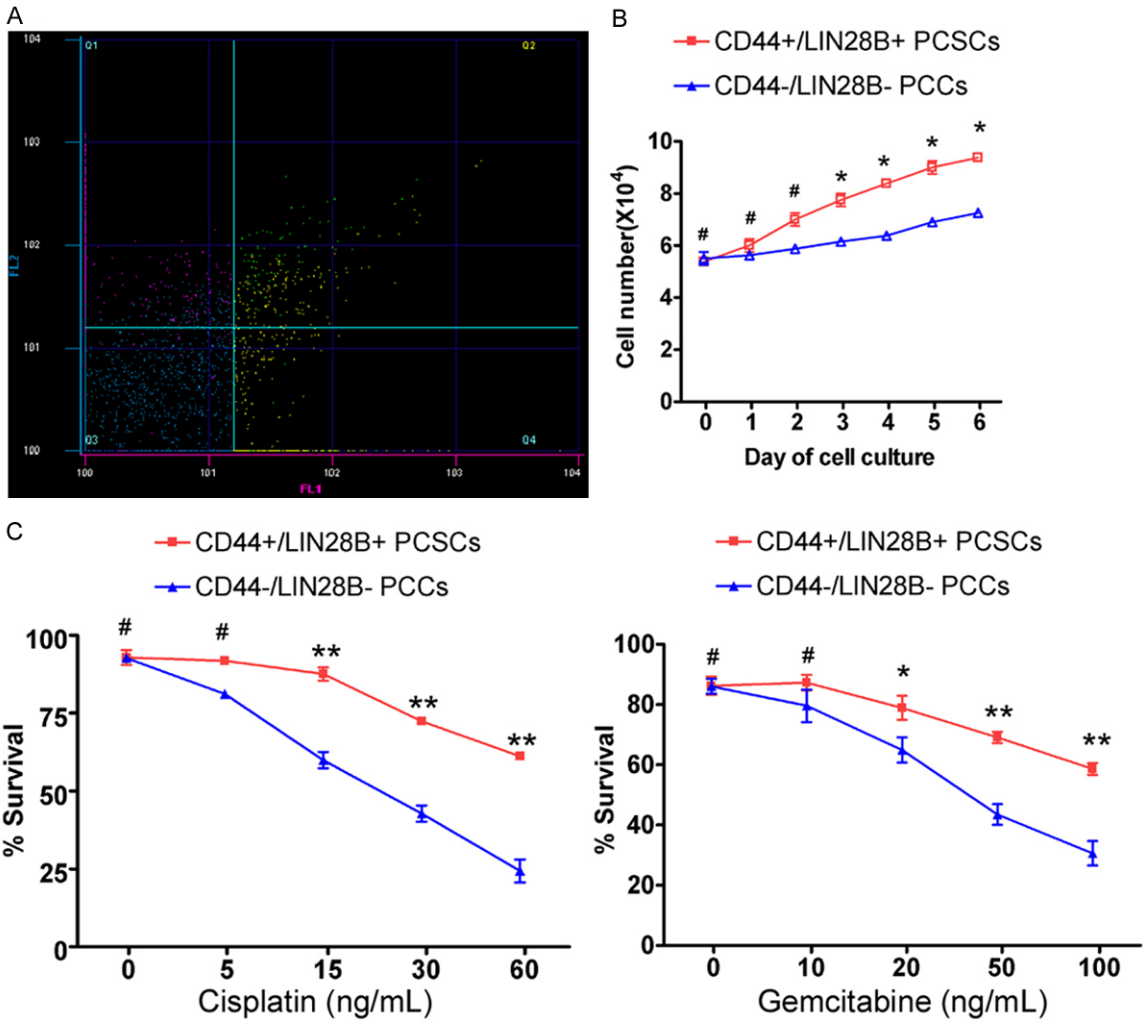

Figure 1. Isolation and characterization of CD44+/LIN28B+ cell multi-drug resistance. A. Flow cytometric analysis of the number of pancreatic cells from primary tumor cells from four human pancreatic cancer tissues expressing CD44 and LIN28B. B. Mean numbers of CD44+/LIN28B+ PCSCs and CD44-/LIN28B- PCCs on days 1-6 after passage. $^{*}P < 0.05$; $^{\#}P > 0.05$ *vs*. PCCs ($n = 3$). C. MTT assay results of the effect of cisplatin and gemcitabine hydrochloride on CD44+/LIN28B+ PCSCs and CD44-/LIN28B-PCCs; $^{**}P < 0.01$; $^{\#}P > 0.05$ *vs*. PCCs ($n = 3$).

total population (**Figure 1**). These results demonstrated that CD44+/LIN28B+ cells, although very exiguous, could be successfully enriched using magnetic-activated cell sorting. The PCSC and PCC proliferation rates were examined on days 1-6 after passage. All measurements were repeated in triplicate. There was no significant difference in the number of cells in the two groups on days 0-2 ($P > 0.05$ *vs*. PCCs; *t*-tests; $n = 3$; **Figure 1**). However, between days 3 and 6, PCSCs divided significantly more rapidly than PCCs ($P < 0.05$ *vs*. PCCs; *t*-tests; $n = 3$). In addition, the inhibitory rates of cisplatin (0, 5, 15, 30, and 60 ng/mL) and gemcitabine hydrochloride (0, 10, 20, 50, and 100 ng/mL) were measured using the MTT proliferation assay to evaluate PCSC and PCC multi-drug resistance. Cisplatin and gemcitabine hydrochloride inhibited both PCSC and PCC growth. However, PCSCs were significantly less susceptible to the cytotoxic effects of both drugs (**Figure 1**). Thus, PCSCs were more resistant to cisplatin and gemcitabine hydrochloride than PCCs, suggesting that the CD44+/LIN28B+ subpopulation may be resistant to a broad spectrum of chemotherapeutics.

CD44+/LIN2B+ PCSCs overexpressed stem cell markers

We used quantitative reverse transcription-PCR (qRT-PCR) to compare the relative gene

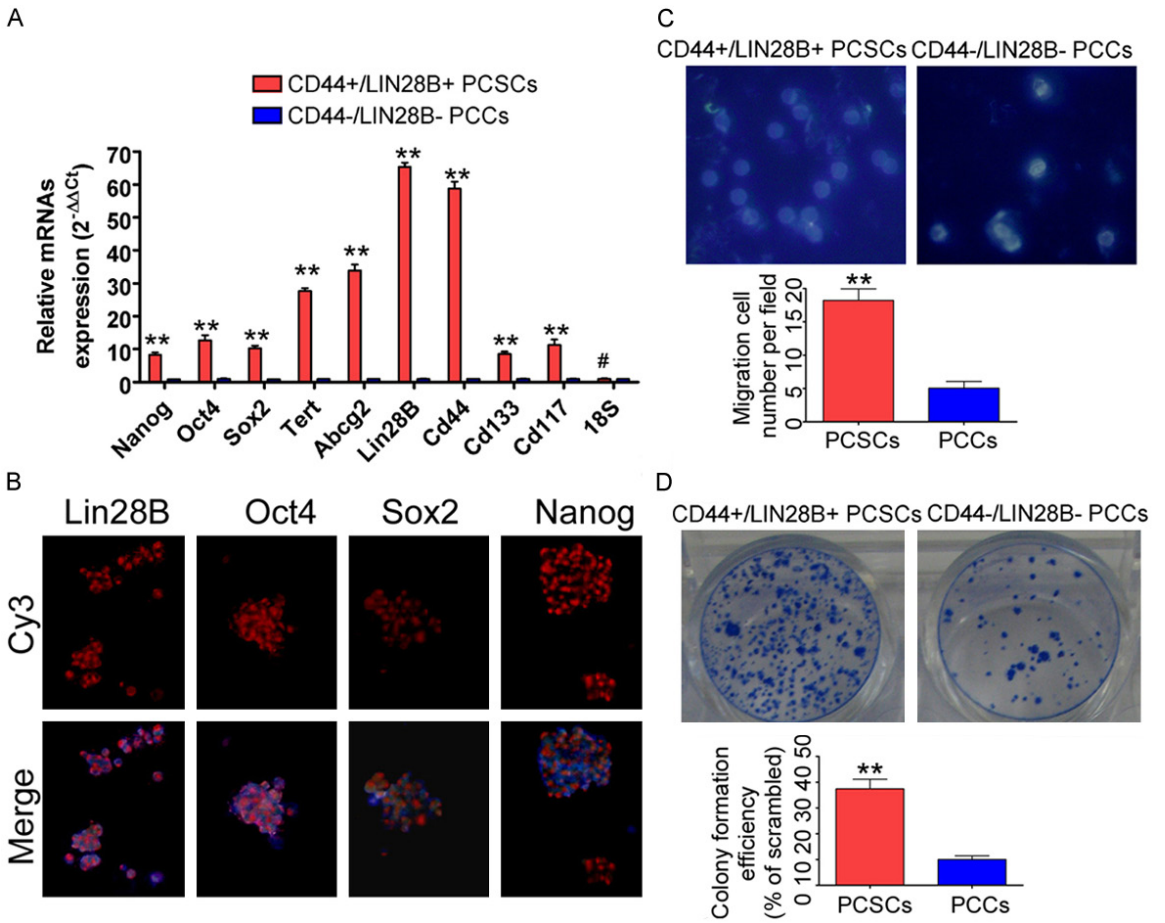

Figure 2. Increased stem cell marker expression and invasion ability in CD44+/LIN28B+ PCSCs compared to CD44-/LIN28B- PCCs. A. QRT-PCR analysis of the relative expression levels of stem cell marker genes in PCSCs and PCCs; $^{**}P < 0.01$; $^{\#}P > 0.05$ *vs*. PCCs ($n = 3$). B. IF of NANOG, SOX2, OCT4, and LIN28B in PCSCs and PCCs; original magnification × 200. C. Transwell assays of PCSCs and PCCs; $^{**}P < 0.01$; $^{\#}P > 0.05$ *vs*. PCCs ($n = 3$). D. Soft agar colony formation assays of PCSCs and PCCs plated at low density; $^{**}P < 0.01$; $^{\#}P > 0.05$ *vs*. PCCs ($n = 3$).

expression levels of several stem cell markers in PCSCs and PCCs; 18S rRNA was used as the internal control. *NANOG*, *OCT4*, *SOX2*, *TERT*, *ABCG2*, *LIN28B*, *CD44*, *CD133*, and *CD117* expression were all significantly higher in PCSCs than in PCCs (**Figure 2**). Immunofluorescence staining (IF) confirmed that PCSCs expressed higher levels of the stem cell markers LIN28B, OCT4, SOX2, and NANOG than PCCs ($P < 0.01$ *vs*. PCCs; *t*-tests; $n = 3$; **Figure 2**). These results suggested that the CD44+/LIN28B+ subpopulation possesses stem cell characteristics.

CD44+/LIN2B+ PCSCs possessed increased migratory and invasive ability

The ability of PCSCs and PCCs to migrate and invade was determined using the Transwell migration assay and soft agar colony formation assay, respectively (**Figure 2**). The Transwell assay revealed that significantly fewer PCCs invaded compared to PCSCs (invading cell numbers: PCSCs, 18 ± 2 *vs*. PCCs, 5 ± 1; $P < 0.01$ *vs*. PCCs; *t*-tests; $n = 3$). The soft agar colony formation assay indicated that PCCs formed substantially fewer colonies when plated at low density than PCSCs (colony formation efficiency: PCCs, 37.40% ± 3.71% *vs*. PCSCs, 10.05% ± 1.39%; $P < 0.01$ *vs*. PCCs; *t*-tests; $n = 3$).

CD44+/LIN2B+ PCSCs induced tumor growth in vivo

To evaluate the tumorigenic capacity of PCSCs and PCCs, 1×10^4 cells were inoculated subcutaneously into athymic nude mice. Tumors were visible in the PCSC-inoculated mice after 1 month. However, PCC-inoculated mice did not

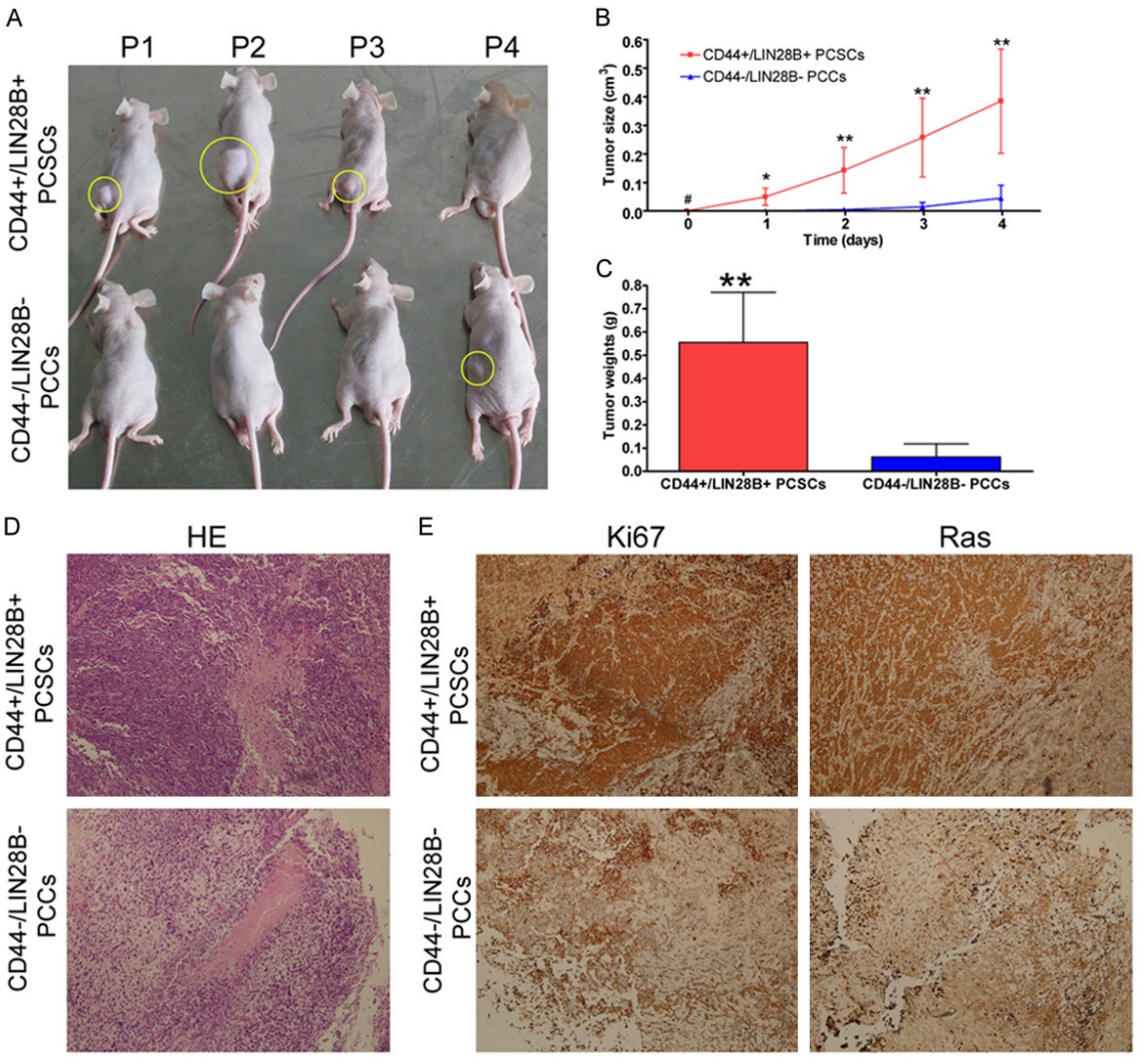

Figure 3. Increased *in vivo* tumor formation ability in CD44+/LIN28B+ PCSCs compared to CD44-/LIN28B- PCCs. CD44+/LIN28B+ PCSCs or CD44-/LIN28B- PCCs were subcutaneously inoculated into severe combined immunodeficient (SCID) mice to form *in vivo* xenografts. A. Representative images of mice with xenograft tumors; yellow rings indicate tumor tissues. B. Tumor growth delay. Tumors formed by the CD44-/LIN28B- PCCs grew more slowly; $^{**}P < 0.01$, $^{*}P < 0.05$, and $^{\#}P > 0.05$ *vs*. PCSC group ($n = 4$). C. Tumor weight; $^{**}P < 0.01$ *vs*. PCSC group ($n = 4$). D. HE staining of PCSC and PCC tumors revealing cellular heterogeneity of the tumors; original magnification × 200. E. Immunohistochemical staining of the cell proliferation markers Ki67 and Ras indicating weakly positive staining in PCSC tumors and positive or strongly positive staining in PCC tumors; original magnification × 200.

exhibit detectable tumors at the same time point (**Figure 3**). Very small tumors were detected in PCC-injected mice after three months. When the mice were sacrificed four months after injection, the tumors formed by PCSCs were significantly heavier than that formed by PCCs ($P < 0.05$ *vs*. PCCs; *t*-tests; $n = 4$). The cell proliferation-related protein Ki-67 was analyzed in tumor sections using immunohistochemistry. The tumors formed by PCSCs displayed positive or strongly positive Ki-67 staining; those formed by PCCs exhibited only weak Ki-67 immunoreactivity (**Figure 3**). These results were the same as that of RAS protein expression (**Figure 3**). Representative hematoxylin and eosin (HE)-stained sections of all subcutaneous xenograft tumors derived from CD44+/LIN28B+ PCSCs were categorized as moderately or poorly differentiated human pancreatic carcinoma (**Figure 3**). Taken together, the *in vivo* xenograft model indicated that low numbers of the CD44+/LIN28B+ subpopulation have the potential to initiate tumor growth. On the other hand, the results showed that

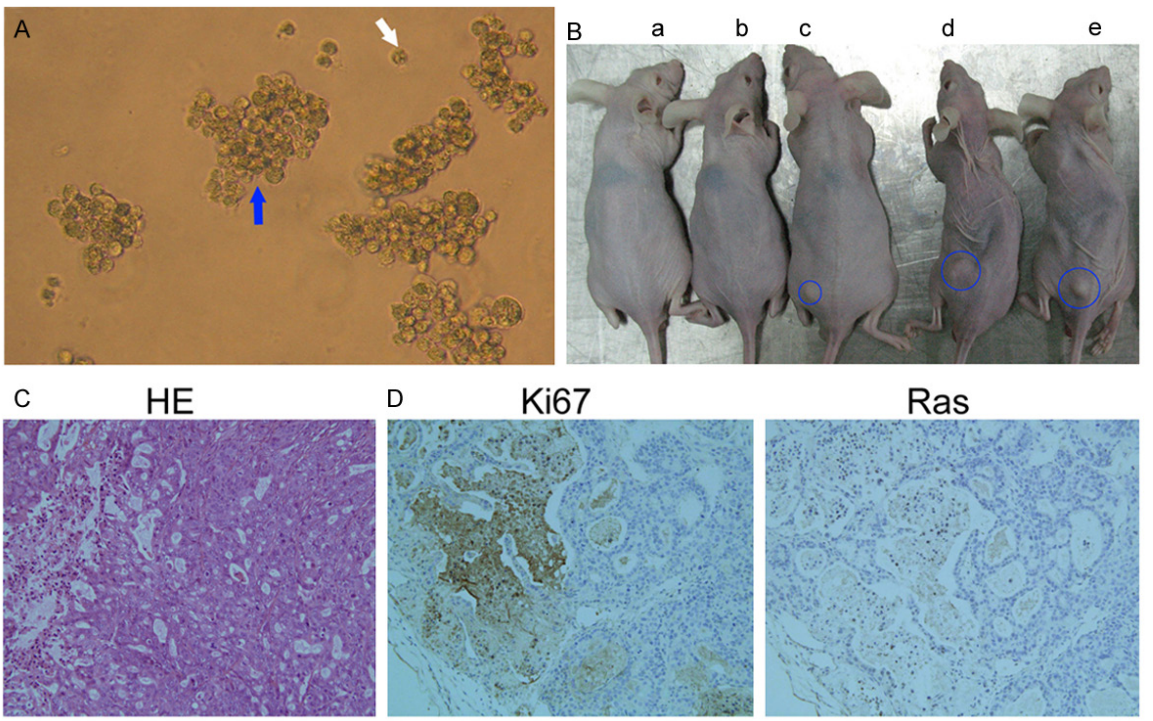

Figure 4. Tumor sphere assay and limiting dilution transplantation assays *in vitro* and *in vivo*. A. Tumor sphere assay *in vitro*. The CD44+/LIN28B+ human PCSCs were formatted non-adherent and non-symmetric cell clones in day 3 after plating. Blue arrow indicated the sphere cell clone; the white arrow indicated the single cell. original magnification × 200. B. The limiting dilution transplantation assays *in vivo*. All CD44+/LIN28B+ human PCSCs were divided into 5 groups, each group was about 1 × 10 cells (a), 1×10^2 cells (b), 1×10^3 cells (c), 1×10^4 cells (d), and 1×10^5 cells (e). Each group cells were inoculated *s.c* in athymic nude mice, respectively. C. HE staining of PCSC tumors revealing cellular heterogeneity of the tumors; original magnification × 200. D. Immunohistochemical staining of the cell proliferation markers Ki67 and Ras indicating positive staining in PCSC tumors; original magnification × 200.

CD44+/LIN28B+ human PCSCs were formatted sphere cells in day 3 after plating (**Figure 4**). These populations were non-adherent and non-symmetric cell clones. When spheres were enzymatically dissociated to single cells, they could give rise to spheres again. This procedure could be repeated, and the sphere proliferated faster than the cells under differentiating conditions. Then, the limiting dilution transplantation assay was used to determine the ability to cause tumor of CD44+/LIN28B+ human PCSCs. All CD44+/LIN28B+ human PCSCs were divided into 5 groups, each group was about 1 × 10 cells, 1×10^2 cells, 1×10^3 cells, 1×10^4 cells, and 1×10^5 cells. Each group cells were inoculated *s.c* in athymic nude mice, respectively. After 1 month, very small tumors were detected in 1×10^3 cells PCSCs-injected mice. But, the tumor derived from 1×10^4 cells PCSCs-injected mice or 1×10^5 cells PCSCs-injected mice was larger significantly than above tumor. However, neither 1 × 10 cells PCSCs-injected mice nor 1×10^2 cells PCSCs-injected mice exhibited detectable tumors at the same time point (**Figure 4**). There assays revealed that the quantitative dependence of PCSCs oncogenicity *in vivo*.

Microarray analysis of cDNA expression patterns of CD44+/LIN28B+ PCSCs and CD44-/LIN28B- PCCs

To evaluate the difference in gene expression patterns of CD44+/LIN28B+ PCSCs and CD44-/LIN28B- PCCs, we prepared a CapitalBio human mRNA microarray V2.0 containing 35000 oligonucleotide probes complementary to known mammalian gene cDNA. Significance microarray analysis and a fold-change criterion (log10 [PCSCs/PCCs] ratio) of > 2 and *q*-value < 0.01 were used to identify significant differences. Using these criteria, we identified 1456 gene mRNAs that were differentially expressed in the PCSCs *vs.* PCCs [among them, 50 gene mRNAs were upregulated (**Table 1**); 139 gene mRNAs were downregulated (**Table 2**)]. Notably,

Table 1. Upregulated expression genes

Genbank Accession	Gene Symbol	Gene Name	Ratio = Log[(PCSCs/PCCs)] (Ratio > 2)
NM_001004317	LIN28B	lin-28 homolog B (C. elegans)	3.151903885
NM_002364	MAGEB2	melanoma antigen family B, 2	3.03093709
NM_017410	HOXC13	homeobox C13	2.951947556
NM_000523	HOXD13	homeobox D13	2.757556259
NM_138815	DPPA2	developmental pluripotency associated 2	2.710770922
NM_001008	RPS4Y1	ribosomal protein S4, Y-linked 1	2.702608074
NM_004405	DLX2	distal-less homeobox 2	2.636932885
NM_173553	TRIML2	tripartite motif family-like 2	2.624075551
NM_001008223	C1QL4	complement component 1, q subcomponent-like 4	2.622575612
NM_021796	PLAC1	placenta-specific 1	2.621359161
NM_006237	POU4F1	POU class 4 homeobox 1	2.612859931
NM_033176	NKX2-4	NK2 homeobox 4	2.583539063
NM_031896	CACNG7	calcium channel, voltage-dependent, gamma subunit 7	2.538431113
NM_001039567	RPS4Y2	ribosomal protein S4, Y-linked 2	2.537580073
NM_031959	KRTAP3-2	keratin associated protein 3-2	2.497118083
NM_001004339	ZYG11A	zyg-11 homolog A (C. elegans)	2.430087357
NM_006546	IGF2BP1	insulin-like growth factor 2 mRNA binding protein 1	2.427697184
NM_002302	LECT2	leukocyte cell-derived chemotaxin 2	2.378282143
NM_153426	PITX2	paired-like homeodomain 2	2.373912239
NM_024016	HOXB8	homeobox B8	2.370713213
BC041859	LOC780529	uncharacterized LOC780529	2.345185492
NM_012159	FBXL21	F-box and leucine-rich repeat protein 21 (gene/pseudogene)	2.297666083
NM_021192	HOXD11	homeobox D11	2.259208887
NM_015557	CHD5	chromodomain helicase DNA binding protein 5	2.250969281
NM_175868	MAGEA6	melanoma antigen family A, 6	2.239072235
NM_018057	SLC6A15	solute carrier family 6 (neutral amino acid transporter), member 15	2.204335394
NM_001112704	VAX1	ventral anterior homeobox 1	2.196077489
NM_001135254	PAX7	paired box 7	2.190715712
NM_005249	FOXG1	forkhead box G1	2.184094348
NM_000853	GSTT1	glutathione S-transferase theta 1	2.176253033
BC039509	LOC643401	uncharacterized LOC643401	2.159535507
NM_025218	ULBP1	UL16 binding protein 1	2.154874271
NM_007129	ZIC2	Zic family member 2	2.118906696
NM_021571	CARD18	caspase recruitment domain family, member 18	2.102380764
NM_003317	NKX2-1	NK2 homeobox 1	2.102375865
NM_016358	IRX4	iroquois homeobox 4	2.101351184
NM_021954	GJA3	gap junction protein, alpha 3, 46kDa	2.098052216
NM_024885	TAF7L	TAF7-like RNA polymerase II, TATA box binding protein (TBP)-associated factor, 50kDa	2.094765437
NM_021240	DMRT3	doublesex and mab-3 related transcription factor 3	2.090471549
NM_001122665	DDX3Y	DEAD (Asp-Glu-Ala-Asp) box polypeptide 3, Y-linked	2.089953594
NM_001004441	ANKRD34B	ankyrin repeat domain 34B	2.08759533
NM_182767	SLC6A15	solute carrier family 6 (neutral amino acid transporter), member 15	2.086853364
NM_203486	DLL3	delta-like 3 (Drosophila)	2.083388477
NM_152739	HOXA9	homeobox A9	2.057843835
NM_004988	MAGEA1	melanoma antigen family A, 1 (directs expression of antigen MZ2-E)	2.043918381
NM_006361	HOXB13	homeobox B13	2.018953044
NM_018712	ELMOD1	ELMO/CED-12 domain containing 1	2.018650868
NM_003108	SOX11	SRY (sex determining region Y)-box 11	2.011435863
NM_024017	HOXB9	homeobox B9	2.001178387

the scatter plot analysis of the gene mRNA microarray results (scatter plot depicts log10-transformed ratios obtained from PCSCs mRNA hybridization *vs*. PCCs mRNA hybridization) indicated differing expression of a certain number of mRNAs between PCSCs *vs*. PCCs (**Figure 5**).

Table 2. Downregulated expression genes

Genbank Accession	Gene Symbol	Gene Name	Ratio = Log[(PCSCs/PCCs)] (Ratio > 2)
NM_001906	CTRB1	chymotrypsinogen B1	4.253352655
NM_001869	CPA2	carboxypeptidase A2 (pancreatic)	4.114128823
NM_001871	CPB1	carboxypeptidase B1 (tissue)	4.073897547
NM_006507	REG1B	regenerating islet-derived 1 beta	3.98556258
NM_001007240	GP2	glycoprotein 2 (zymogen granule membrane)	3.957646381
NM_000936	PNLIP	pancreatic lipase	3.941809299
NM_001008387	REG3G	regenerating islet-derived 3 gamma	3.809492882
NM_006217	SERPINI2	serpin peptidase inhibitor, clade I (pancpin), member 2	3.726041579
NM_007352	CELA3B	chymotrypsin-like elastase family, member 3B	3.721707666
NM_005747	CELA3A	chymotrypsin-like elastase family, member 3A	3.679697239
NM_019617	GKN1	gastrokine 1	3.650917342
NM_182536	GKN2	gastrokine 2	3.608465143
NM_015849	CELA2B	chymotrypsin-like elastase family, member 2B	3.387080468
NM_007352	CELA3B	chymotrypsin-like elastase family, member 3B	3.37675489
NM_002909	REG1A	regenerating islet-derived 1 alpha	3.339716528
NM_198998	AQP12A	aquaporin 12A	3.332356441
NM_033440	CELA2A	chymotrypsin-like elastase family, member 2A	3.216462824
NM_001285	CLCA1	chloride channel accessory 1	3.186337576
NM_000928	PLA2G1B	phospholipase A2, group IB (pancreas)	3.176664135
NM_007272	CTRC	chymotrypsin C (caldecrin)	3.133808678
NM_001443	FABP1	fatty acid binding protein 1, liver	3.10178095
NM_001041	SI	sucrase-isomaltase (alpha-glucosidase)	3.077879399
NM_001633	AMBP	alpha-1-microglobulin/bikunin precursor	3.043261652
NM_000477	ALB	albumin	3.001962782
NM_014276	RBPJL	recombination signal binding protein for immunoglobulin kappa J region-like	2.973692081
NM_019010	KRT20	keratin 20	2.961282952
NM_001040462	BTNL8	butyrophilin-like 8	2.925304863
NM_001868	CPA1	carboxypeptidase A1 (pancreatic)	2.908065427
NM_001040105	MUC17	mucin 17, cell surface associated	2.885213886
NM_000349	STAR	steroidogenic acute regulatory protein	2.868034449
NM_014471	SPINK4	serine peptidase inhibitor, Kazal type 4	2.847637265
NM_178161	PTF1A	pancreas specific transcription factor, 1a	2.840800222
NM_001145643	PHGR1	proline/histidine/glycine-rich 1	2.807670721
NM_144696	AXDND1	axonemal dynein light chain domain containing 1	2.794013389
NM_152321	ERP27	endoplasmic reticulum protein 27	2.783485155
NM_001644	APOBEC1	apolipoprotein B mRNA editing enzyme, catalytic polypeptide 1	2.779192438
NM_017625	ITLN1	intelectin 1 (galactofuranose binding)	2.774310879
NM_007272	CTRC	chymotrypsin C (caldecrin)	2.756421395

NM_005588	MEP1A	meprin A, alpha (PABA peptide hydrolase)	2.720645656
NM_005747	CELA3A	chymotrypsin-like elastase family, member 3A	2.698310666
NM_003889	NR1I2	nuclear receptor subfamily 1, group I, member 2	2.679493358
NM_032044	REG4	regenerating islet-derived family, member 4	2.675557226
NM_001136485	C11orf86	chromosome 11 open reading frame 86	2.673767266
NM_001832	CLPS	colipase, pancreatic	2.671370467
NM_006229	PNLIPRP1	pancreatic lipase-related protein 1	2.670896325
NM_000492	CFTR	cystic fibrosis transmembrane conductance regulator (ATP-binding cassette sub-family C, member 7)	2.663599825
NM_005459	GUCA1C	guanylate cyclase activator 1C	2.642911633
NM_003465	CHIT1	chitinase 1 (chitotriosidase)	2.629621307
NM_001076	UGT2B15	UDP glucuronosyltransferase 2 family, polypeptide B15	2.629470167
NM_170741	KCNJ16	potassium inwardly-rectifying channel, subfamily J, member 16	2.592859069
NM_032044	REG4	regenerating islet-derived family, member 4	2.582210072
NM_001907	CTRL	chymotrypsin-like	2.578185726
NM_001807	CEL	carboxyl ester lipase (bile salt-stimulated lipase)	2.564669478
NM_138938	REG3A	regenerating islet-derived 3 alpha	2.540410193
NM_005621	S100A12	S100 calcium binding protein A12	2.507022164
NM_152491	PM20D1	peptidase M20 domain containing 1	2.473104564
NM_001086	AADAC	arylacetamide deacetylase (esterase)	2.467135126
NM_003225	TFF1	trefoil factor 1	2.463144163
NM_001003811	TEX11	testis expressed 11	2.450551531
NM_000111	SLC26A3	solute carrier family 26, member 3	2.44439235
NM_003296	CRISP2	cysteine-rich secretory protein 2	2.440968817
NM_002443	MSMB	microseminoprotein, beta-	2.434490133
NM_005621	S100A12	S100 calcium binding protein A12	2.424419104
NM_000253	MTTP	microsomal triglyceride transfer protein	2.423321574
NM_001039112	FER1L6	fer-1-like 6 (C. elegans)	2.406190944
NM_005495	SLC17A4	solute carrier family 17 (sodium phosphate), member 4	2.398680041
NM_001080538	AKR1B15	aldo-keto reductase family 1, member B15	2.396507273
NM_032787	GPR128	G protein-coupled receptor 128	2.381097185
NM_002153	HSD17B2	hydroxysteroid (17-beta) dehydrogenase 2	2.366343469
NM_001185	AZGP1	alpha-2-glycoprotein 1, zinc-binding	2.365710298
NM_006229	PNLIPRP1	pancreatic lipase-related protein 1	2.363652616
NM_016369	CLDN18	claudin 18	2.34702268
NM_001216	CA9	carbonic anhydrase IX	2.344158438
NM_002181	IHH	Indian hedgehog	2.334859325
NM_005420	SULT1E1	sulfotransferase family 1E, estrogen-preferring, member 1	2.33310927
NM_170736	KCNJ15	potassium inwardly-rectifying channel, subfamily J, member 15	2.326162651
NM_020299	AKR1B10	aldo-keto reductase family 1, member B10 (aldose reductase)	2.3217617
NM_020299	AKR1B10	aldo-keto reductase family 1, member B10 (aldose reductase)	2.321622661
NM_021969	NR0B2	nuclear receptor subfamily 0, group B, member 2	2.295677518

NM_005423	TFF2	trefoil factor 2	2.283895997
NM_001101404	SH2D7	SH2 domain containing 7	2.275404367
NM_019596	C21orf62	chromosome 21 open reading frame 62	2.275342284
NM_004212	SLC28A2	solute carrier family 28 (sodium-coupled nucleoside transporter), member 2	2.271658804
NM_005814	GPA33	glycoprotein A33 (transmembrane)	2.269666309
NM_005950	MT1G	metallothionein 1G	2.263322944
NM_033050	SUCNR1	succinate receptor 1	2.258936505
NM_001074	UGT2B7	UDP glucuronosyltransferase 2 family, polypeptide B7	2.257942574
NM_014080	DUOX2	dual oxidase 2	2.251638427
NM_007193	ANXA10	annexin A10	2.24536539
NM_080870	DPCR1	diffuse panbronchiolitis critical region 1	2.227683528
NM_153343	ENPP6	ectonucleotide pyrophosphatase/phosphodiesterase 6	2.212974443
NM_001080468	SYCN	syncollin	2.205592389
NM_002927	RGS13	regulator of G-protein signaling 13	2.204853321
NM_198477	CXCL17	chemokine (C-X-C motif) ligand 17	2.202850396
NM_001080405	CEACAM18	carcinoembryonic antigen-related cell adhesion molecule 18	2.20198379
NM_001721	BMX	BMX non-receptor tyrosine kinase	2.200051762
NM_000384	APOB	apolipoprotein B (including Ag(x) antigen)	2.199449748
NM_005951	MT1H	metallothionein 1H	2.196296242
NM_000128	F11	coagulation factor XI	2.195335353
NM_001073	UGT2B11	UDP glucuronosyltransferase 2 family, polypeptide B11	2.194853528
NM_003963	TM4SF5	transmembrane 4 L six family member 5	2.194043134
NM_000341	SLC3A1	solute carrier family 3 (cystine, dibasic and neutral amino acid transporters, activator of cystine, dibasic and neutral amino acid transport), member 1	2.19054256
NM_007072	HHLA2	HERV-H LTR-associating 2	2.186569068
NM_001169	AQP8	aquaporin 8	2.185414667
NM_006061	CRISP3	cysteine-rich secretory protein 3	2.174405317
NM_004063	CDH17	cadherin 17, LI cadherin (liver-intestine)	2.169387832
NM_024743	UGT2A3	UDP glucuronosyltransferase 2 family, polypeptide A3	2.163743137
NM_170736	KCNJ15	potassium inwardly-rectifying channel, subfamily J, member 15	2.156444411
NM_021161	KCNK10	potassium channel, subfamily K, member 10	2.135896894
NM_001080527	MYO7B	myosin VIIB	2.135028806
NM_138969	SDR16C5	short chain dehydrogenase/reductase family 16C, member 5	2.117283297
NM_203395	IYD	iodotyrosine deiodinase	2.109420053
NM_194439	RNF212	ring finger protein 212	2.108893597
NM_001085382	PSAPL1	prosaposin-like 1 (gene/pseudogene)	2.106102812
NM_004132	HABP2	hyaluronan binding protein 2	2.105420932
NM_001807	CEL	carboxyl ester lipase (bile salt-stimulated lipase)	2.104908892
NM_001040105	MUC17	mucin 17, cell surface associated	2.103367532
NM_003015	SFRP5	secreted frizzled-related protein 5	2.102989014
NM_006418	OLFM4	olfactomedin 4	2.092198248
NM_004963	GUCY2C	guanylate cyclase 2C (heat stable enterotoxin receptor)	2.087387429

NM_001010903	C6orf222	chromosome 6 open reading frame 222	2.083954408
NM_145650	MUC15	mucin 15, cell surface associated	2.077301731
NM_002639	SERPINB5	serpin peptidase inhibitor, clade B (ovalbumin), member 5	2.076055664
NM_000277	PAH	phenylalanine hydroxylase	2.075090795
NM_014465	SULT1B1	sulfotransferase family, cytosolic, 1B, member 1	2.068579425
NM_206819	MYBPC1	myosin binding protein C, slow type	2.057838856
NM_001079807	PGA3	pepsinogen 3, group I (pepsinogen A)	2.047264536
NM_207581	DUOXA2	dual oxidase maturation factor 2	2.042660099
NM_080658	ACY3	aspartoacylase (aminocyclase) 3	2.037460662
NM_152311	CLRN3	clarin 3	2.036559534
NM_001010857	LELP1	late cornified envelope-like proline-rich 1	2.033215345
NM_182983	HPN	hepsin	2.028306399
NM_024533	CHST5	carbohydrate (N-acetylglucosamine 6-O) sulfotransferase 5	2.027032681
NM_005379	MYO1A	myosin IA	2.024188703
NM_024921	POF1B	premature ovarian failure, 1B	2.020794379
NM_212557	AMTN	amelotin	2.017073209
NM_003226	TFF3	trefoil factor 3 (intestinal)	2.013612065
NM_000035	ALDOB	aldolase B, fructose-bisphosphate	2.011105368

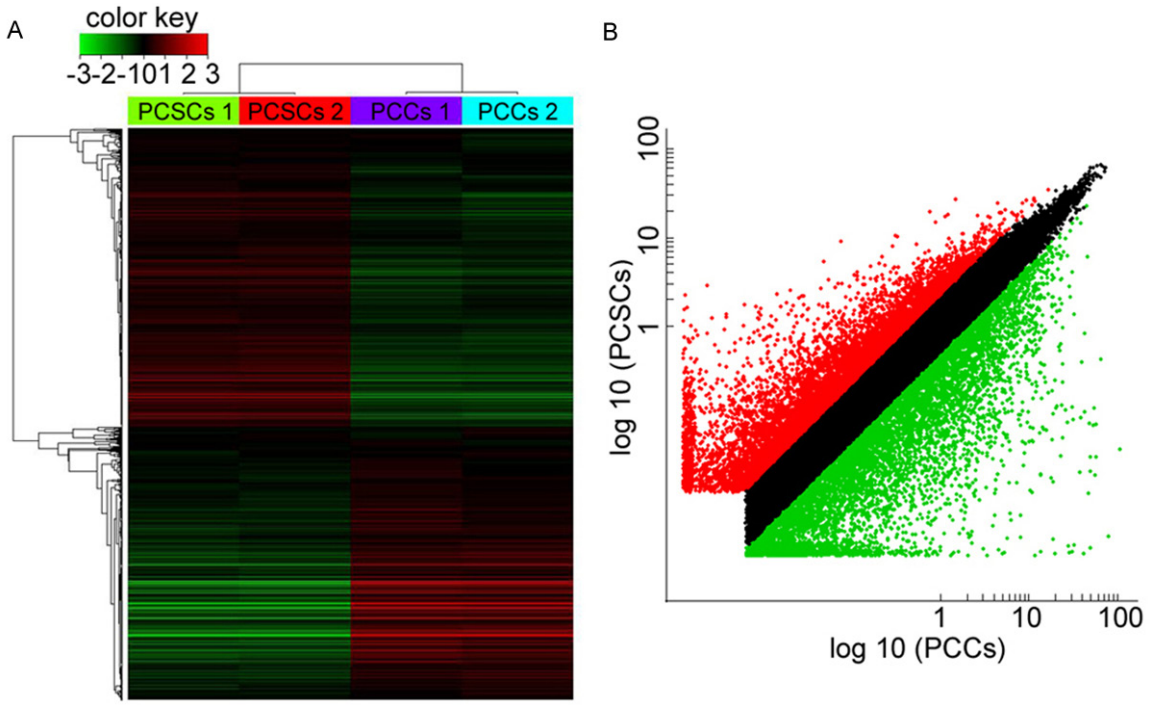

Figure 5. Microarray analysis of cDNA expression patterns in CD44+/LIN28B+ PCSCs *vs*. CD44-/LIN28B- PCCs. A. Cluster analysis of differentially expressed gene mRNAs in CD44+/LIN28B+ PCSCs *vs*. CD44-/LIN28B- PCCs. B. Scatter plot indicating differing mRNA expression between CD44+/LIN28B+ PCSCs *vs*. CD44-/LIN28B- PCCs.

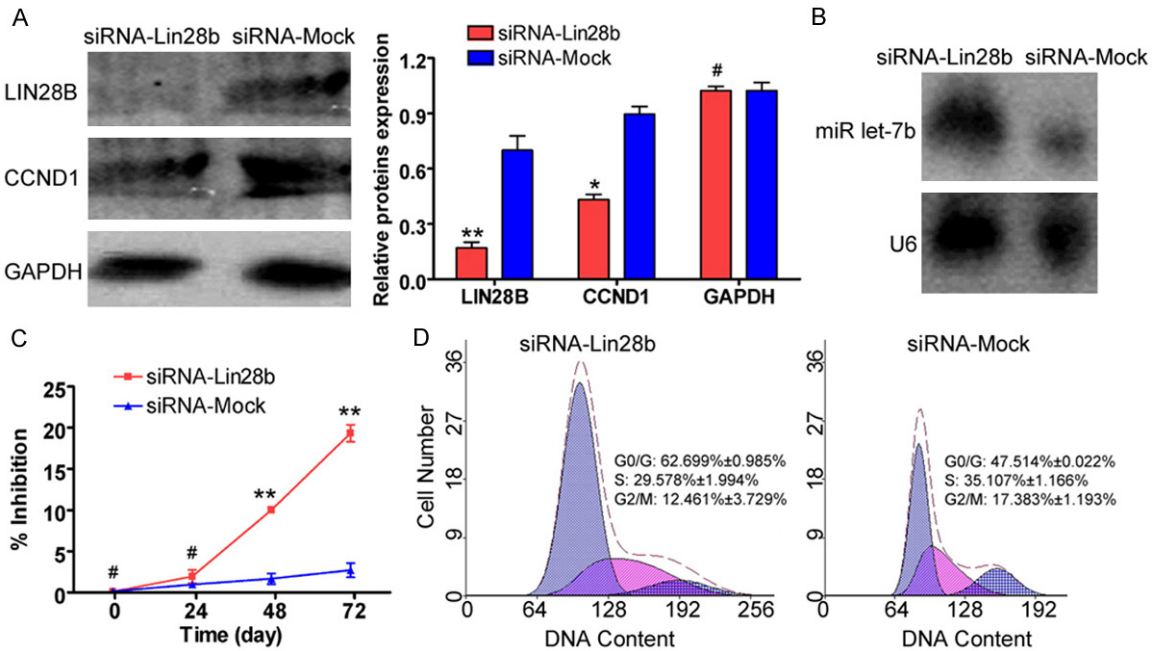

Figure 6. Suppression of LIN28B expression in CD44+/LIN2B+ PCSCs decreased proliferation while stimulating let-7b expression to interfere with CCND1 expression. A. Western blotting confirming that CCND1 expression was significantly decreased in siRNA-LIN28B–transfected PCSCs compared to siRNA-Mock-transfected PCSCs. Glyceraldehyde-3-phosphate dehydrogenase (GAPDH) was used as a loading control; $^{**}P < 0.01$, $^{*}P < 0.05$, and $^{\#}P > 0.05$ *vs*. siRNA-Mock ($n = 3$). B. Northern blotting indicating a strong let-7b hybridization signal in siRNA-LIN28B-transfected PCSCs compared to siRNA-Mock-transfected PCSCs. C. MTT assay of the effect of proliferation inhibition in siRNA-LIN28B-transfected PCSCs compared to siRNA-Mock-transfected PCSCs; $^{**}P < 0.01$, $^{\#}P > 0.05$ *vs*. siRNA-Mock; ($n = 3$). D. FCM showing that compared to siRNA-Mock-transfected cells, siRNA-LIN28B-transfected PCSCs were arrested in the G0/G1 phase and the percentage of S-phase cells was significantly decreased.

These results demonstrate that gene mRNA expression patterns in PCSCs were significantly different from that of PCCs.

Suppression of endogenous LIN28B expression in CD44+/LIN2B+ PCSC decreased proliferation while stimulating let-7b expression to interfere with CCND1 expression

To determine whether endogenous *LIN28B* interfered with expression of the promoter miRNA let-7b and influenced CD44+/LIN2B+ PCSC proliferation, siRNA-LIN28B and siRNA-Mock were transfected into CD44+/LIN2B+ PCSCs. The efficiency of the transfected siRNA on mRNA and protein expression was detected by western and northern blotting, respectively. Western blotting (**Figure 6**) showed that LIN28B and CCND1 expression in PCSCs transfected with siRNA-Mock (0.700 ± 0.078; 0.897 ± 0.041, respectively) was higher than that in PCSCs transfected with siRNA-LIN28B (0.170 ± 0.031; 0.433 ± 0.027, respectively; $P < 0.05$ *vs*. siRNA-Mock; *t*-tests*;* $n = 3$). These results demonstrated that siRNA-LIN28B specifically interfered with LIN28B expression in PCSCs; at the same time, it weakened CCND1 expression. Northern blotting revealed a strong let-7b hybridization signal in PCSCs transfected with siRNA-LIN28B compared with PCSCs transfected with siRNA-Mock (**Figure 5**). To determine whether LIN28B interference would suppress PCSC proliferation, inhibition at 0, 24, 48, and 72 h was measured by MTT assay (**Figure 6**). At 48 h and 72 h, PCSCs transfected with siRNA-Mock were significantly less susceptible to the proliferation inhibitory effect than PCSCs transfected with siRNA-LIN28B ($P < 0.01$ *vs*. siRNA-Mock; *t*-tests*;* $n = 3$; **Figure 6**). FCM demonstrated significant cell cycle arrest of PCSCs transfected with siRNA-LIN28B. Compared with PCSCs transfected with siRNA-Mock, PCSCs transfected with siRNA-LIN28B were arrested in the G0/G1 phase and the percentage of S-phase cells was significantly decreased ($P < 0.05$ *vs*. siRNA-Mock; *t*-tests*;* $n = 3$; **Figure 6**). These data indicate that not only was endogenous let-7b expression promoted and CCND1 inhibited in the CD44+/LIN28B+ PCSCs, but also that proliferation of the subpopulation was weakened when endogenous LIN28B was suppressed.

Discussion

Since pancreatic CSCs were first found in pancreatic cancer tissue, it was generally believed that they were closely associated with both high proliferation and invasion ability, and difficult early-stage diagnosis and poor recurrence-free prognosis. However, knowledge of the biological characteristics of PCSCs is limited. Although it has been reported that the CD31+/CD45+, Hoechst 33342-/CD133+/ALDH1+, ESA+/CD44+, and CD24+/CD44+ subpopulations in pancreatic cancer not only overexpress stem cell markers [1, 3, 4, 6, 12], but also exhibit high self-renewal and migratory ability and multi-drug resistance, we believe that there are other subpopulations that possess PCSC characteristics in primary pancreatic cancer tissues. Referring to previous studies, we found that LIN28B regulated not only embryonic stem cells, but also cancer cell self-renewal. When exogenous LIN28 was overexpressed in host cells, the proliferation ability in these cells increased significantly. This indicates that LIN28B is a positive regulator of cell proliferation. As CD44 expression occurs in a wide variety of CSCs, we used CD44 and LIN28B as CSC markers to sort PCSCs from primary pancreatic cancer cells. Although the CD44+/LIN28B+ subpopulation share in the overall cell population was very low, it exists at a certain ratio in the tumor tissues of many pancreatic cancer patients. We determined the CSC characteristics of CD44+/LIN28B+ and CD44-/LIN28B- pancreatic cancer cells. We found that not only self-renewal ability, but also migratory ability and multi-drug resistance were higher in CD44+/LIN28B+ cells than in CD44-/LIN28B- cells. Moreover, there was high expression of stem cell markers by CD44+/LIN28B+ cells, and the cells exhibited high tumorigenic ability *in vivo*. In view of these results, we believe that the CD44+/LIN28B+ subpopulation in pancreatic cancer cells also possesses PCSC characteristics.

The other reason for using LIN28B as a PCSC sorting marker is that it regulates OCT4 expression in CSCs. Qiu and Huang [26] reported that LIN28 mediated post-transcriptional regulation of OCT4 expression in human embryonic stem cells. They found that LIN28 binds *OCT4* mRNA directly through high-affinity sites within its coding region and that interaction between LIN28 and RNA helicase A may play a part in the observed regulation. They further demonstrated that decreasing RNA helicase A levels impaired LIN28-dependent stimulation of translation in a reporter system [26]. In view of many reports demonstrating that CSCs also

overexpress stem cell markers, such as OCT4, SOX2, and NANOG, we hypothesized that pancreatic cancer cells expressed high levels of stem cell markers, such as the LIN28B-overexpressing subpopulation. Our findings demonstrated that stem cell marker expression in CD44+/LIN28B+ PCSCs was significantly higher than that in CD44-/LIN28B- cells.

In conclusion, CD44+/LIN28B+ PCSCs not only express high levels of stem cell markers, but also possess strong self-renewal and migratory ability and multi-drug resistance *in vitro* and are tumorigenic *in vivo*.

Acknowledgements

This work was supported by grant from National Natural Science Foundation of China (No. 81202811), and Project funded by China Postdoctoral Science Foundation (No. 2014-M550250), and Shanghai Municipal Health Bureau Fund (No. 20124320) to Te Liu.

Disclosure of conflict of interest

None.

Address correspondence to: Drs. Dayong Jin and Weiqi Lu, Department of General Surgery, Zhongshan Hospital, Fudan University, Shanghai 200032, China. Tel: 86-21-64041990; Fax: 86-21-64038038; E-mail: jindayo@163.com; Te Liu, Shanghai Geriatric Institute of Chinese Medicine, Longhua Hospital, Shanghai University of Traditional Chinese Medicine, Building C, 365 Xiangyang Road, Shanghai 200031, China. Tel: 86-21-64720010; Fax: 86-21-64720010; E-mail: teliu79@126.com

References

[1] Wang X, Liu Q, Hou B, Zhang W, Yan M, Jia H, Li H, Yan D, Zheng F, Ding W, Yi C, Hai W. Concomitant targeting of multiple key transcription factors effectively disrupts cancer stem cells enriched in side population of human pancreatic cancer cells. PLoS One 2013; 8: e73942.

[2] Siegel R, Naishadham D, Jemal A. Cancer statistics, 2012. CA Cancer J Clin 2012; 62: 10-29.

[3] Herreros-Villanueva M, Zhang JS, Koenig A, Abel EV, Smyrk TC, Bamlet WR, de Narvajas AA, Gomez TS, Simeone DM, Bujanda L, Billadeau DD. SOX2 promotes dedifferentiation and imparts stem cell-like features to pancreatic cancer cells. Oncogenesis 2013; 2: e61.

[4] Han JB, Sang F, Chang JJ, Hua YQ, Shi WD, Tang LH, Liu LM. Arsenic trioxide inhibits viability of pancreatic cancer stem cells in culture and in a xenograft model via binding to SHH-Gli. Onco Targets Ther 2013; 6: 1129-1138.

[5] Lu Y, Zhu H, Shan H, Lu J, Chang X, Li X, Lu J, Fan X, Zhu S, Wang Y, Guo Q, Wang L, Huang Y, Zhu M, Wang Z. Knockdown of Oct4 and Nanog expression inhibits the stemness of pancreatic cancer cells. Cancer Lett 2013; 340: 113-123.

[6] Li C, Heidt DG, Dalerba P, Burant CF, Zhang L, Adsay V, Wicha M, Clarke MF, Simeone DM. Identification of pancreatic cancer stem cells. Cancer Res 2007; 67: 1030-1037.

[7] Liu T, Xu F, Du X, Lai D, Liu T, Zhao Y, Huang Q, Jiang L, Huang W, Cheng W, Liu Z. Establishment and characterization of multi-drug resistant, prostate carcinoma-initiating stem-like cells from human prostate cancer cell lines 22RV1. Mol Cell Biochem 2010; 340: 265-273.

[8] Ponti D, Costa A, Zaffaroni N, Pratesi G, Petrangolini G, Coradini D, Pilotti S, Pierotti MA, Daidone MG. Isolation and in vitro propagation of tumorigenic breast cancer cells with stem/progenitor cell properties. Cancer Res 2005; 65: 5506-5511.

[9] Reya T, Morrison SJ, Clarke MF, Weissman IL. Stem cells, cancer, and cancer stem cells. Nature 2001; 414: 105-111.

[10] Marx J. Cancer research. Mutant stem cells may seed cancer. Science 2003; 301: 1308-1310.

[11] Pardal R, Clarke MF, Morrison SJ. Applying the principles of stem-cell biology to cancer. Nat Rev Cancer 2003; 3: 895-902.

[12] Van den Broeck A, Vankelecom H, Van Delm W, Gremeaux L, Wouters J, Allemeersch J, Govaere O, Roskams T, Topal B. Human pancreatic cancer contains a side population expressing cancer stem cell-associated and prognostic genes. PLoS One 2013; 8: e73968.

[13] Bapat SA, Mali AM, Koppikar CB, Kurrey NK. Stem and progenitor-like cells contribute to the aggressive behavior of human epithelial ovarian cancer. Cancer Res 2005; 65: 3025-3029.

[14] Park DM, Rich JN. Biology of glioma cancer stem cells. Mol Cells 2009; 28: 7-12.

[15] Lei XX, Xu J, Ma W, Qiao C, Newman MA, Hammond SM, Huang Y. Determinants of mRNA recognition and translation regulation by Lin28. Nucleic Acids Res 2012; 40: 3574-3584.

[16] Moss EG, Tang L. Conservation of the heterochronic regulator Lin-28, its developmental expression and microRNA complementary sites. Dev Biol 2003; 258: 432-442.

[17] Peng S, Chen LL, Lei XX, Yang L, Lin H, Carmichael GG, Huang Y. Genome-wide studies reveal that Lin28 enhances the translation of genes important for growth and survival of

human embryonic stem cells. Stem Cells 2011; 29: 496-504.
[18] Xu F, Wang H, Zhang X, Liu T, Liu Z. Cell proliferation and invasion ability of human choriocarcinoma cells lessened due to inhibition of Sox2 expression by microRNA-145. Exp Ther Med 2013; 5: 77-84.
[19] Qin W, Ren Q, Liu T, Huang Y, Wang J. MicroRNA-155 is a novel suppressor of ovarian cancer-initiating cells that targets CLDN1. FEBS Lett 2013; 587: 1434-1439.
[20] Liu T, Huang Y, Liu J, Zhao Y, Jiang L, Huang Q, Cheng W, Guo L. MicroRNA-122 influences the development of sperm abnormalities from human induced pluripotent stem cells by regulating TNP2 expression. Stem Cells Dev 2013; 22: 1839-1850.
[21] Cheng W, Liu T, Wan X, Gao Y, Wang H. MicroRNA-199a targets CD44 to suppress the tumorigenicity and multidrug resistance of ovarian cancer-initiating cells. FEBS J 2012; 279: 2047-2059.
[22] Zhang L, Liu T, Huang Y, Liu J. microRNA-182 inhibits the proliferation and invasion of human lung adenocarcinoma cells through its effect on human cortical actin-associated protein. Int J Mol Med 2011; 28: 381-388.
[23] Xu B, Zhang K, Huang Y. Lin28 modulates cell growth and associates with a subset of cell cycle regulator mRNAs in mouse embryonic stem cells. RNA 2009; 15: 357-361.
[24] Schultz J, Lorenz P, Gross G, Ibrahim S, Kunz M. MicroRNA let-7b targets important cell cycle molecules in malignant melanoma cells and interferes with anchorage-independent growth. Cell Res 2008; 18: 549-557.
[25] Yu F, Yao H, Zhu P, Zhang X, Pan Q, Gong C, Huang Y, Hu X, Su F, Lieberman J, Song E. let-7 regulates self renewal and tumorigenicity of breast cancer cells. Cell 2007; 131: 1109-1123.
[26] Qiu C, Ma Y, Wang J, Peng S, Huang Y. Lin28-mediated post-transcriptional regulation of Oct4 expression in human embryonic stem cells. Nucleic Acids Res 2010; 38: 1240-1248.